Paleoclimatic Registers from Semi-arid Costal Sediments of Southeastern India: A Multi Proxy Approach

Anburaj Vidyasakar, Helena Sant'Ovaia, Linto Alappat, P. Morthekai, Seshachalam Srinivasalu, A.K. Singhvi, Ferreira Jorge and Celeste Gomes

Abstract The red sand dunes appear along the south east, -west coast of Tamil Nadu, India between the latitudes and longitudes of 8°07′56″N to 8°22′11″N; 77° 19′84″E to 77°53′40″E. The dune sands from this region were studied through magnetic methods such as magnetic susceptibility measurements and acquisition of isothermal remanent magnetization, geochemistry and X-ray diffraction methods. Optically stimulated luminescence (OSL) dating method was used to constrain the chronology of deposits. Three sections were excavated up to 5–9.5 m with one inland deposit (TPV) and two near coastal sections (THOP and MUT).

Celeste Gomes—deceased

A. Vidyasakar (✉) · S. Srinivasalu
Department of Geology, Faculty of Science and Humanities,
Anna University, Chennai, India
e-mail: a.vidyasakar@gmail.com

A. Vidyasakar · H. Sant'Ovaia
Pole of the Faculty of Sciences, Earth Sciences Institute,
Rua do Campo Alegre, Porto 4169-007, Portugal

L. Alappat
Department of Geology and Environmental Science,
Christ College, Irinjalakuda 680125, Kerala, India

P. Morthekai
Luminescence Dating Laboratory, Birbal Sahni Institute of Palaeobotany,
53 University Road, Lucknow 226007, India

A.K. Singhvi
Planetary and Geoscience Division, Physical Research Laboratory,
Ahmedabad 380009, India

F. Jorge
LaboratórioNacional de Energia e Geologia, I.P/Rua da Amieira, Apartado 1089,
S. Mamede de Infesta, Porto 4466-901, Portugal

C. Gomes
CGUC, Department of Earth Sciences, Faculty of Sciences and Technology,
University of Coimbra, Largo Marquês de Pombal, Coimbra 3000-272, Portugal

© Springer International Publishing AG 2017

O. Abdalla et al. (eds.), *Water Resources in Arid Areas: The Way Forward*,
Springer Water, DOI 10.1007/978-3-319-51856-5_1

a.vidyasakar@gmail.com

The magnetic parameters show both significant contribution of hematite structures and indicate the presence of multi-domain magnetite or mixed mineral contents of magnetite and anti-ferromagnetic minerals in the sample. The occurrence of magnetite in THOP and TPV sections is possibly due to the marine sediments transported by sturdy onshore winds. In XRD data, correlation analysis indicated TPV and MUT sections have a similar type of deposition and THOP did not show any positive correlation with TPV and MUT and even with its own deposition. In comparison with geochemistry data, χ variation and OSL dates, it was shown that the sample MUT21 (200 cm) with an OSL age of 14 ± 2 ka indicated deposition during the humid interval and at $\sim 17 \pm 2$ to $\sim 19 \pm 2$ ka MUT61 (600 cm) depicts the dry period of deposition.

Keywords Magnetic parameters · X-ray diffraction · Optically stimulated luminescence · Geochemistry · Teri sands · Hematite · Magnetite

1 Introduction

The environmental changes in a region may happen due to climatic variability or as a result of human intervention, which usually lasts for an extended period. Moreover, research on various aspects preceding the climate change suggested that climatic variability has occurred sporadically in the past, notably through a quaternary period in response to different forcing's, e.g., orbital variations and solar activity changes (insolation) (Wolff et al. 2010; Sanchez Goñi and Harrison 2010). It is to be noted that a change in the climate disturbs the coastal areas around the globe causing changes in sea level. Therefore, in the context of Quaternary climate change, it is ideal to study sediment archives along the coast. The study may hold substantial evidence of coastline advance and retreat in adherence to past variations regarding sea level and its landscape response (e.g., Islam and Tooley 1999; Alappat et al. 2015; Brückner (1988, 1989)). Also, reconstruction of the paleo-sea level is a long and intricate process. Hence, it involves reminiscing the fragments of evidence left in nature, recording of those fragments through dating of the event in question and final interpretation of available data (Morner 2010). The red dunes on the southeast coast of India is a potential terrestrial archive of climate change and provide vital information about the landscape response to such variations. Red dunes are referred to as 'teri sands or teris' in the literature and are categorized as inland, coastal and teri (near-coastal) dunes by earlier researchers (Joseph et al. 1997, 1999). According to the standard Tamil dictionary, teri means 'a heap of sand.' Some researchers (Jayangondaperumal et al. 2012) used the term 'wasteland' because the local people deemed it as useless for agriculture.

The foremost intent of the present study is to draw a distinct line between previous dry and wet climatic intervals using various proxies like magnetic studies, Optically Stimulated Luminescence (OSL) dating, X-ray Diffraction (XRD) and geochemical analysis. The soil magnetic parameters are relatively quick and easy to

a.vidyasakar@gmail.com

obtain information compared to geochemical, sedimentological and paleontological data. It is helpful in obtaining information about a broad range of climatic and environmental changes (Maher and Thompson 1999). OSL dating has the number of advantages as a chronological tool in coastal environments over other methods, considering its wide dating range, direct dating of events and provides ages in calendar years (Jacobs et al. 2008). It also includes the use of most abundant minerals like quartz and feldspar as dosimeters for age determination, which makes its wide application in the majority of terrestrial sedimentary archives. The qualitative analysis of sediments has been carried out to define major and minor constituent minerals present in the samples collected at different depths in the coastal area by XRD technique. The geochemical analysis of samples can be of greater help in understanding the sediment dynamics underlying behind a particular geological system (Albarède 2003).

2 Study Area

The study area is located in the southwest and southeast coast of Tamil Nadu, India between the latitudes and longitudes of 8°07′56″N to 8°22′11″N; 77°19′84″E to 77°53′40″E. Three representative sections were excavated in the area as indicated in Fig. 1, viz-a-viz; Muttom (MUT; 8°07′56″N, 77°19′84″E), Thopuvilla (THOP; 8°19′57″N, 77°57′27″E) and Edayanvilai (TPV; 8°22′11″N, 77°53′40″E). The various morphological settings from east and west coast will be further discussed in the following section. At Muttom, Thopuvilla and Edayanvilai, a 9.5, 7.4 and 4 m sections respectively were excavated to reach up to the palaeo-surface.

2.1 Regional Climate

The study area falls under the semi- arid and subtropical climatic conditions. Muttom, Thoppuvillai and Edayanvillai receive most of its rainfall during the summer (during SW monsoon). The climate has been classified according to Koppen and Geiger climate classification as Aw (Peetal et al. 2007). In Muttom, the average annual precipitation is 1093 mm and the variation in precipitation between the wettest and driest month is 178 mm. The average temperature in Muttom is recorded as 29 °C. The lowest average annual temperature in the year occurs in December when it is around 26 °C. In Thopuvillai and Edayanvillai average annual rainfall is 729 mm, and among the wettest and driest months, the change in precipitation is 199 mm. With an average temperature of ∼31 °C, May is the hottest month of the year with a mean maximum of 38 °C. The coldest month is the January, with temperatures averaging 26.2 °C (www.climate-data.org).

a.vidyasakar@gmail.com

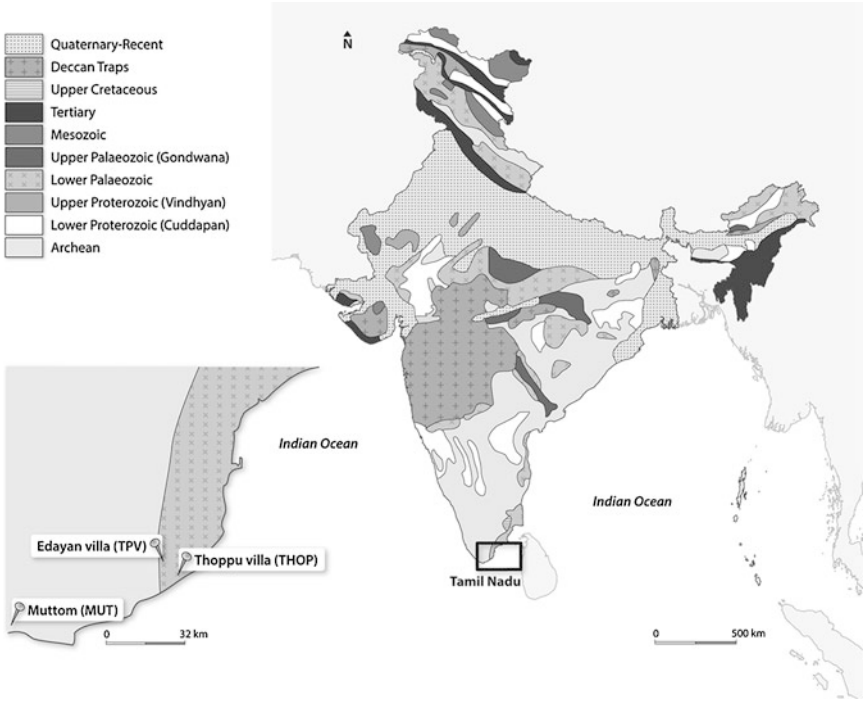

Fig. 1 Map of the study area with sample location in southeast-southwest coast of India

2.2 Regional Stratigraphy and Geomorphology

The teri sands in the area cover an area of up to $\sim$500 km^2 and thickness at places reach up to $\sim$12 m (Gardner 1986). The igneous and metamorphic rocks that found below ovari series are from Archean period. The Pleistocene coastal sediments (Ovari Series) sits on Archaean granulitic rocks, most of which are peninsular gneiss, garnet-sillimanite-graphite gneiss and charnockite gneiss (Jayangondaperumal et al. 2012). Idindakarai Series (Fig. 2) overlies the Ovari Series and comprises terrigenous grains of gravel and sand size and shell fragments of shallow marine origin (Jayangondaperumal et al. 2012). The Kanyakumari Series that superimposes on Idindakarai Series consist of fossil coastal dunes concreted with calcium carbonate sediments and also with marine sediments. (Jayangondaperumal et al. 2012). In addition to that, Poochikkadu Series is covered with calcrete and some marine sediments (Jayangondaperumal et al. 2012). The Inland teri sands found in big patches are dark in colour and discontinuous, while coastal teri sands are continuous and light coloured. Marine deposits of Mandapam Series overlie the teri deposits (Jayangondaperumal et al. 2012). Along the shoreward direction, teri sands rest on either of the crystalline basement, the Ovari marine sandstone, aeolianite of

a.vidyasakar@gmail.com

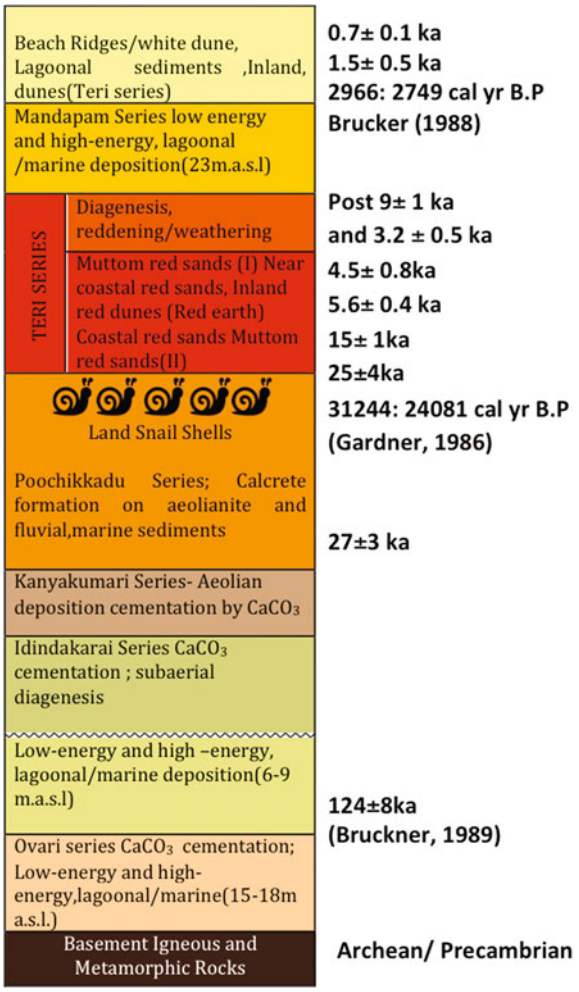

Fig. 2 Regional stratigraphy from Jayangondaperumal et al. (2012) and some modified ages from Allapat et al. (2013a, b)

Kanyakumari or Poochikkadu Series (Gardner 1986; Joseph et al. 1997). Perceiving sediment texture Joseph et al. (1997), inferred that teri sediments were originated from the wide-open continental shelf during a phase of low relative sea level, and these deposits were transported by high landward winds. According to chandrasekharan and Murugan (2001) sands are rich in heavy minerals like ilmenite, rutile, zircon, garnet, monazite and sillimanite, suggest their source from Precambrian Khondalite, charnockites and granite gneisses rocks.

The geology of the area comprises Archaean granulitic rocks, predominantly peninsular gneiss (garnet-sillimanite-graphite gneiss) and charnockite gneiss (Alappatet al. 2013a, b). The littoral area has Pleistocene and recent fluvial, fluviomarine and marine deposits (Alappat et al. 2013a, b). The rocks of Mio-Pliocene

a.vidyasakar@gmail.com

age (early Neogene) namely Cuddalore formation, is exposed towards the northeast at Muttom. Also, at Muttom the red sands occur as a dune against a headland into the Arabian Sea. This landscape is bounded by recent dunes, beach ridges, swales and beaches towards the coast and unveils badland topography with weathering and gully erosion subjecting up to $\sim$10–12 m thick sand unit at its central part. The red sands overlie laterized country rock with a slope towards SE. Moreover, dunes on the east coast are cut by some rivers and streams. River Valliyar joins the Arabian Sea at the northwest side of this cape cutting across the dunes at the coast. Some discontinuous coast, parallel lagoons and swales separate the near coastal dunes. The floodplains of rivers restrict the dune development as discontinuous patches (Alappat et al. 2013a, b).

3 Methodology

3.1 Field Work and Sample Collection

Three profiles were excavated in the southeast and southwest coast using mechanical excavators and number of trench sections were made at different levels to collect the required samples. In general, the sections were excavated in areas were the thickness of the loose, incoherent sand is less than 1 m thick to reach up to the older sand units by omitting the recent reactivated sand at places. The samples for magnetic susceptibility, textural and geochemical analyses were collected at 10 cm intervals along vertical profiles and were carefully packed in sample bags and labeled for laboratory analyses. Some OSL samples was collected from different units having distinct stratigraphic relations. Samples for OSL dating was collected in 10 $\times$ 2 in. aluminum tubes and was sealed light tight immediately after sample collection.

3.2 Laboratory Analyses

3.2.1 Geochemical Analysis

According to Saravanan (2012, p. 43) the samples were dried in a hot air furnace at 60 °C to eliminate the moisture and 100 g of samples were taken by repeated coning and quartering to obtain a homogeneous representative sample. The following procedures were performed:

(i) *Clay fraction removal*: The samples were soaked in water with 2 g of sodium hexametaphosphate ($(NaPO_3)_6$) overnight and then washed in water (325 sieve mesh) to eliminate the clay portions. The samples were weighed and weight loss was taken as the weight of clay.

a.vidyasakar@gmail.com

(ii) *Organic matter removal*: The samples were treated with hydrogen peroxide (H_2O_2) overnight, and rinsed with water (325 sieve mesh) until a clear column of water without any turbidity was achieved. The samples were then dried and weighed, and weight loss was taken as the weight of the organic material.

(iii) *Carbonate removal*: The samples were treated with 10% hydrochloric acid (HCl) to the carbonates in the sediments. After washing and drying, the samples were weighed, and the weight loss was taken as the weight of carbonates.

(iv) *Iron removal*: The samples were treated with 10% nitric acid (HNO_3) over night and were then washed (325 sieve mesh) with water until a clear column of water was achieved. The samples were then dried and weighed and the weight loss was taken as the weight of Fe.

(v) *Grain size analyses*: The grain size may have an impact in accordance with heavy mineral composition, usually fine-to-medium grained sand yield the optimum heavy mineral assemblages. Sieving was carried out in ASTM at the 1/2Φ interval. The sieve sets are stacked in descending order with respect to their sizes and were shaken using a mechanical sieve shaker continuously for about 20 min. During sieving, proper care was taken to minimize the sand loss from sieve sets. The samples collected on each sieve were taken separately and weights of individual fractions were tabulated. The sieved sands of 80, 100 and 120 meshes were kept separately for heavy mineral studies. It is a basic premise of sedimentology that every sedimentary unit is formed as a result of its response to a certain set of environmental conditions (Blatt et al. 1980). The geochemical analysis has been obtained from Department of Geology, Anna University, Chennai, Tamil Nadu, India.

3.2.2 Magnetic Measurement

To ascertain the strength and type of environmental magnetic carriers in samples, magnetic parameters were measured and scrutinized. Before measuring the low-field magnetic susceptibility, samples were dried at 40 °C and packed in the Department of Geology, Anna University, Chennai, Tamil Nadu, India. Maher (1986) cited the importance of drying samples at low temperature before investigation to evade any possible changes in mineralogy. The specific or mass susceptibility χ (measured in m^3/kg units) is expressed as the ratio of material magnetization and 'J' per mass unit to the weak external magnetic field, H: $J = \chi H$. Magnetic susceptibility has been measured using KLY-4S Kappabridge equipment in Earth Sciences Institute at the University of Porto, Portugal. In order to know whether the instrument is working correctly, a minimum of three susceptibility measurements of each sample was taken, and the average value was used for the study.

a.vidyasakar@gmail.com

The Remanence assimilated by a sample exposed to a direct magnetic field at ambient temperature is termed as Isothermal Remanent Magnetization (IRM). Moreover, IRM has been measured in a minispin fluxgate magnetometer (Molspin Ltd.) after magnetization in a pulse magnetizer (Molspin Ltd.) in the Department of Earth Sciences, University of Coimbra, Portugal. The IRM acquired in the magnetic field of one tesla (T) was defined as Saturation Isothermal Remanent Magnetization (SIRM). Thus, IRM was imparted at fields of 0/12.5/25/50/75/100/150/200/250/300/500/700/900 mT and up to 1000 mT and backfield was imparted up to 1000 mT. To find the relative influence of antiferromagnetic minerals, Hard IRM using the formula $HIRM = 0.5 \times (SIRM + IRM_{-300\ mT})$ (Alargarsamy 2009), wherein $SIRM = IRM_{1T}$ (Lourenco et al. 2012) was calculated and Hard% (= HIRM/SIRM × 100) has been determined (Lourenco et al. 2014). The S-ratio parameters were used to determine the relative contribution of hematite versus magnetite by dividing each IRM value with corresponding value from SIRM ($S_{-100} = |IRM_{-100\ mT}/SIRM|$ and $S_{-300} = |IRM_{-300\ mT}/SIRM|$) (Thompson and Oldfield 1986; Maher and Thompson 1999; Evans and Heller 2003). The SIRM/χ is the ratio between Saturation Isothermal Remanent Magnetization and magnetic susceptibility.

3.2.3 X-ray Diffraction Analysis

The mineral composition was determined in non-oriented powder mounts for bulk sample analysis. In addition to that, XRD measurements with Pro Alfa 1 equipment were made at Laboratório Nacional de Energia e Geologia, I.P. The samples used for magnetic measurements were used for the XRD measurements. The selected samples have undergone coning and quartering to ensure they are homogeneous to evade errors during XRD analysis. The estimates of mineral abundances were based on subsequent peak intensities. Hence, for semi-quantification of identified principal clay minerals, peak areas of specific reflections were calculated and weighed (Lapa and Reis 1977). Finally, High Score Plus software was used to correct the intensities and to correlate between each sample in the present study through adopting Pan Analytical X'Pert Pro Alfa1 model, which is 200 times precision-centric and faster than old models. This X-ray Diffraction model requires minimum 4 grams sample with the grain size of 400–450 mesh is kept as the ideal of a sediment sample. Samples are nicely grained and powder mounts are prepared with back loading firm pressure. In this X-ray Diffraction model, Copper tube is used with the wavelength of 1.541874 Å and goniometer radius of 240 mm. The samples analysis time take is 15 s per step.

3.2.4 Optically Stimulated Luminescence (OSL)

The OSL dating was used to reveal the characteristics of coastal deposits from various geographical and geological settings and to study the relationship between

a.vidyasakar@gmail.com

periods of sediment accretion and environmental change. During the collection of OSL dating samples, the samples were protected from the sunlight exposure using thick black blankets (Fig. 3). OSL dating was carried out at Physical Research Laboratory, Ahmedabad, Gujarat, India. The selected cores were sampled and processed under controlled red light laboratory conditions for luminescence studies. The superficial 1.5 cm were not sampled to prevent possible contamination of bleached and/or disturbed outer parts while retrieving the core. The quartz grain fractions of 100–150 μm or 150–200 μm used from every sample were separated using the standard laboratory preparation procedure and dry sieving (Aitken 1998). Thus, after extracting the grain size of 100–200 μm, samples were treated with 0.1 N hydrochloric acid (HCl) to remove the presence of carbonates, 0.01 N sodium oxalate ($C_2Na_2O_4$) and 30% hydrogen peroxide (H_2O_2) were used to remove clay coatings as well as to segregate the grains and to remove the organic matter from samples. The quartz-rich fraction (<2.70–2.62 g cm^{-3}) was separated by density separation using an aqueous solution of sodium polytungstate ($3Na_2WO_4\ 9WO_3\ H_2O$). Also, the quartz fraction was etched using 40% hydrofluoric acid (HF) for 60 min to remove feldspar contamination. The HF etching also removed the outermost layer of quartz grains to evade the impact of alpha particles in coarse grain sand. The samples were then washed and neutralized with distilled water and sieved again with respective mesh to get rid off grains that had become smaller. The sieved grains were mounted on stainless steel aliquots in a uniform thin layer and fixed with silicon spray shortly before measurement. The methodological details and SAR protocol optimization of red dune sand are detailed in Alappat et al. (2013a, b).

The single aliquot regenerative dose (SAR) protocol for quartz (Murray and Wintle 2000; Wintle and Murray 2006) was used to determine the equivalent dose of the samples. An automated Riso TL/OSL DA-20 reader attached to a 90Sr/90Y beta source was used for the OSL measurements. The quartz grains were stimulated by a blue light emitting diodes (LED) (470 ± 30 nm). A Hoya U-340 (7.5 mm) filter was placed between the photomultiplier and sample to detect luminescence signals from quartz grains. The dose recovery test at different preheat temperature shows that the given dose was recovered effectively at a preheat temperature of 200 °C with a cut heat of 160 °C. The De values were calculated using signals integrated using the first 0.64 s and an early background was subtracted corresponding to 1.12–2.4 s.

The dose rates were calculated from the activity concentrations of decay chains 238U, 232Th and 40K measured using high-resolution gamma spectrometry (High Purity Germanium (HPGe)) at Physical Research Laboratory, Ahmedabad. The dose-rate conversion factors of Guérin et al. (2011) and beta attenuation factors of Mejdahl (1979) were applied for calculation. The cosmic dose rate was calculated based on the method proposed by Prescott and Hutton (1994).

a.vidyasakar@gmail.com

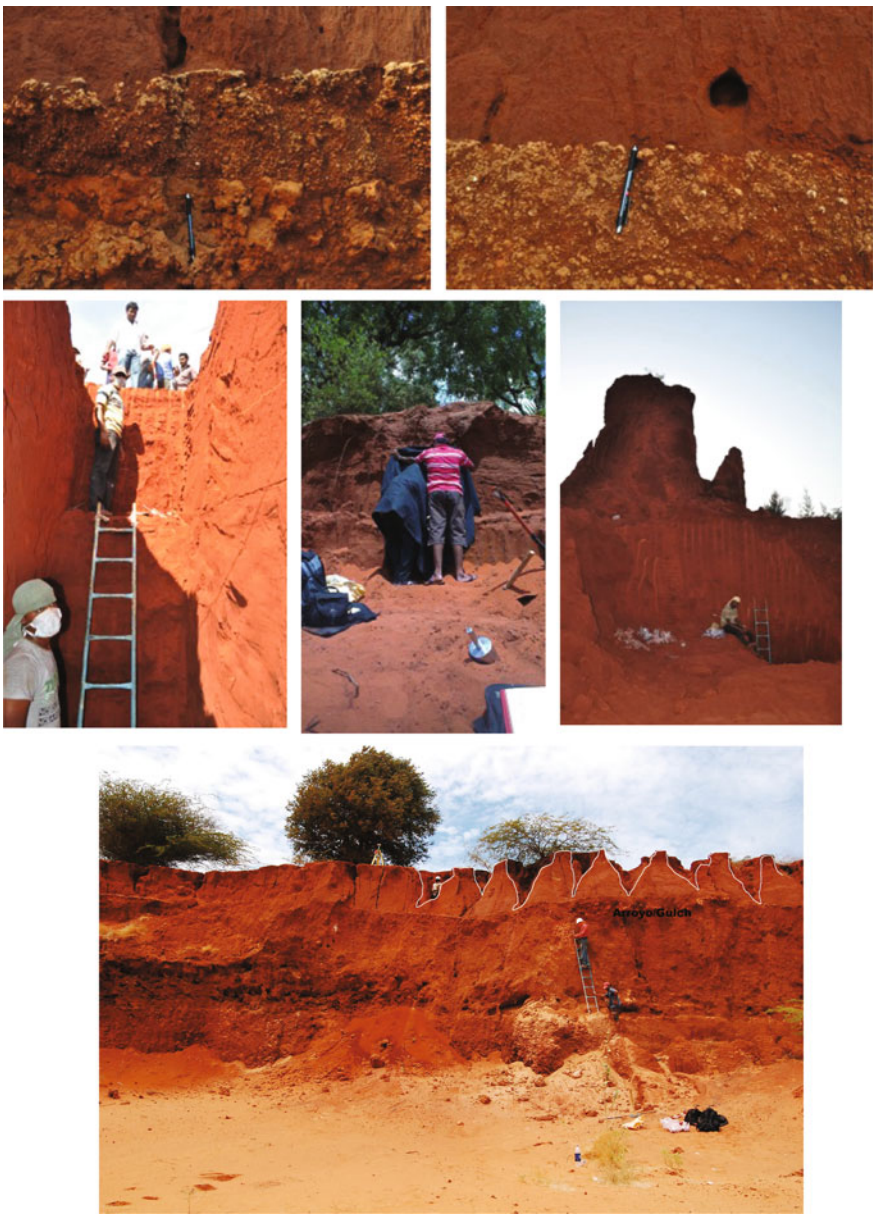

Fig. 3 General view of Teri sands, trench sampling and description how OSL samples are were collected

a.vidyasakar@gmail.com

4 Results

4.1 Magnetic Parameters

The magnetic susceptibility, χ, reflects total mineralogical composition of sediments with an existing contribution from ferromagnetic minerals, which have much higher susceptibility values than paramagnetic and diamagnetic minerals such as clay or quartz (e.g., Verosub and Roberts 1995; Dekkers 1997; Maher and Thompson 1999; Evans and Heller 2003). The χ, SIRM, S-ratios, SIRM/χ and HIRM% variations in the different selection sites for some representative samples of each section were presented in Table 1. In THOP area, magnetic susceptibility values range between 11.67 and 55.16 $\times$ 10^{-8} m^3 kg^{-1} (mean = 36.46) and SIRM between 0.58 and 3.11 $\times$ 10^{-3} A m^2 kg^{-1} (mean = 2.10) (Vidyasakar et al. 2015). In TPV area, magnetic susceptibility values range between 11.31 and 67.40 $\times$ 10^{-8} m^3 kg^{-1} (mean = 54.25) and SIRM between 1.04 and 7.74 $\times$ 10^{-3} A m^2 kg^{-1} (mean = 6.20) (Vidyasakar et al. 2015). In MUT area, magnetic susceptibility values were between 5.66 and 83.76 $\times$ 10^{-8} m^3 kg^{-1} (mean = 34.23) and SIRM between 0.12 and 6.50 $\times$ 10^{-3} A m^2 kg^{-1} (mean = 2.95). According Vidyasakar et al. (2015) in THOP, the S_{-300} (S_{-300} = |$IRM_{-300\ mT}$/SIRM|) close to 1 indicates that the saturation of the magnetization is obtained to a field close to 300 mT, which is typical of a magnetic structure with the magnetic behavior of magnetite. On the other hand, the HIRM% parameter is proportional to the content of hematite. In the case of THOP, the mean value of HIRM is around 10% (lower than in TPV and MUT sections), which indicates the low fraction of hematite-structure. Even so, in the THOP section the sample THOP15 shows a singular magnetic behavior with a low S_{-300} ratio and a high HIRM content, which point out a hematite-structure contribution. At the depth THOP 21 to THOP 31 where we have calcrete formation binded along with dead marine fossil, which reveals the sudden sea level change and the oxidation played important role of hematite contribution.

In TPV and MUT area samples, the absence of or a small amount of magnetite-like structure is substantiated by values of HIRM%, which are always higher than 10%, endorsing the significant contribution of canted antiferromagnetic (hematite) structures. The SIRM/χ ratio depends on the composition and grain size of magnetic particles. Moreover, when the magnetic mineralogy is homogeneous, this ratio revealed changes in the grain size assemblage of ferrimagnetic minerals (Thompson and Oldfield 1986; Moreno et al. 2003). The closer the value of S-300 ratio is to one, the bigger is the contribution of magnetite to magnetic mineralogy and the smaller is the contribution of other iron silicates or iron oxides. This means that the closer the value of S-300 ratio is to one, the higher the homogeneity of magnetic mineralogy is. When comparing THOP, TPV and MUT, the mean ratio of S-300 ratio is higher for THOP section, indicating the higher homogeneity of magnetic mineralogy.

As the magnetic mineralogy indicated by the S_{-300} ratio is not homogeneous in samples from TPV and MUT areas, SIRM/χ ratio only can be considered in THOP

a.vidyasakar@gmail.com

Table 1 Results of magnetic parameters in different profiles

Depth (cm)	Samples	χ ($\times 10^{-8}$ m^3/kg)	SIRM($\times 10^{-3}$ A m^2/kg)	S-300	S-100	HIRM %	SIRM/χ (kA/m)
10	THOP2-L1	52.49	3.08	0.83	0.48	8.34	5.86
50	THOP6-L1	49.38	2.45	0.84	0.48	7.80	4.97
80	THOP9-L1	55.16	2.90	0.77	0.33	11.27	5.26
150	THOP16-L1	41.49	3.11	0.82	0.40	8.81	7.49
170	THOP18-L1	49.51	3.00	0.81	0.40	9.74	6.07
210	THOP22-L1	48.57	2.76	0.80	0.40	9.84	5.69
220	THOP1-L2	11.67	0.58	0.78	0.31	11.09	4.94
260	THOP5-L2	30.81	2.52	0.82	0.44	8.87	8.17
300	THOP9-L2	36.41	1.98	0.83	0.49	8.62	5.43
330	THOP12-L2	30.91	2.30	0.81	0.36	9.69	7.45
360	THOP3-L3	32.34	2.37	0.78	0.25	11.00	7.32
400	THOP7-L3	34.47	2.88	0.73	0.07	13.36	8.36
440	THOP11-L3	27.89	1.68	0.73	0.22	13.36	6.02
480	THOP15-L3	24.53	1.27	0.57	0.23	21.68	5.19
540	THOP21-L3	21.95	1.04	0.80	0.34	9.87	4.75
570	THOP3-L4	39.75	2.06	0.81	0.49	9.68	5.19
590	THOP5-L4	44.74	1.88	0.84	0.52	8.15	4.21
640	TH0P10-L4	35.69	1.54	0.81	0.50	9.40	4.33
670	THOP13-L4	27.90	1.51	0.82	0.47	8.84	5.41
710	THOP17-L4	33.65	1.16	0.82	0.50	9.04	3.44
	Mean	36.47	2.10	0.79	0.38	10.42	5.78
0	TPV-1	57.41	6.55	0.74	0.21	12.99	114.13
40	TPV5	56.72	7.67	0.75	0.15	12.58	13.52
90	TPV10	59.67	6.91	0.77	0.21	11.47	11.59
140	TPV15	55.85	6.56	0.74	0.21	13.14	11.74
230	TPV24	61.24	6.36	0.77	0.23	11.35	10.39
290	TPV30	64.43	6.73	0.76	0.24	11.78	10.45
350	TPV36	67.40	7.74	0.74	0.27	12.76	11.49
400	TPV41	11.31	1.04	0.76	0.25	12.15	9.21
	Mean	54.25	6.20	0.75	0.22	12.28	24.06
0	MUT1	47.60	5.53	0.80	0.32	9.76	11.62
40	MUT5	35.17	4.54	0.76	0.22	12.12	12.91
90	MUT10	29.00	3.41	0.73	0.12	13.60	11.74
150	MUT16	52.77	4.75	0.80	0.36	10.10	9.01
170	MUT18	74.05	6.50	0.84	0.48	7.96	8.78
200	MUT21	28.27	3.57	0.71	0.06	14.57	12.64
230	MUT24	47.15	0.12	0.77	0.30	11.27	10.71
280	MUT29	34.56	3.17	0.72	0.15	13.81	9.16
310	MUT32	22.62	2.65	0.66	0.32	17.12	11.73

(continued)

a.vidyasakar@gmail.com

Table 1 (continued)

Depth (cm)	Samples	χ ($\times 10^{-8}$ m^3/kg)	SIRM($\times 10^{-3}$ A m^2/kg)	S-300	S-100	HIRM %	SIRM/χ (kA/m)
350	MUT36	78.80	5.85	0.86	0.52	7.19	7.43
370	MUT38	19.85	2.16	0.62	0.07	12.15	10.89
390	MUT40	83.76	5.79	0.87	0.51	6.58	6.91
440	MUT45	17.06	1.52	0.57	0.12	21.49	8.89
550	MUT56	12.79	1.05	0.53	0.18	23.46	8.19
680	MUT69	9.73	0.69	0.52	0.17	24.00	7.11
750	MUT76	8.74	0.61	0.51	0.14	24.56	6.99
840	MUT85	8.56	0.73	0.53	0.16	23.65	8.56
940	MUT95	5.66	0.46	0.48	0.18	25.87	8.05
	Mean	34.23	2.95	0.68	0.24	15.51	9.52

THOP and TPV data source from Vidyasakar et al. (2015)

section. According to Thompson and Oldfield (1986) the mean SIRM/χ value of 10 kA m^{-1} indicated a magnetite grain size of 5 µm. However, Sandgren and Thompson (1990) indicated that a value of 6.40 kA m^{-1} corresponded to a magnetite grain size of 8 µm. As stated by these authors, mean SIRM/χ value of 5.78 kA m^{-1} obtained in THOP area samples indicated an average grain size of ferrimagnetic particles of ca. 8 µm in THOP. IRM acquisition curves are necessary to estimate the characteristic coercivity of ferromagnetic structures. The trend of IRM possession curves depends on the relative concentration of low-coercivity in magnetite type minerals and high-coercivity in hematite type minerals respectively (Thompson and Oldfield 1986). In THOP area samples, IRM acquisition curve showed saturation in fields between 500 and 600 mT followed by a small increase in intensity by increased fields, suggesting that these samples may contain both multidomain magnetite structures and antiferromagnetic minerals such as hematite. In MUT and TPV area samples, IRM acquisition curve showed saturation is not obtained at applied fields, which pointed towards the presence of a canted antiferromagnetic phase such as hematite (Fig. 4). The remanence coercivity parameter, B_{OCR} was obtained from IRM curves (Fig. 4). Also, THOP area samples showed B_{OCR} that varies from 50 mT to 75 mT depicting multidomain magnetite or magnetite and antiferromagnetic minerals; other THOP samples present B_{OCR} between 25 mT and 50 mT endorsed that these samples are magnetite bearing (Vidyasakar et al. 2015). In TPV samples, B_{OCR} changing from 50 mT to 75 mT indicated the existence of a multidomain magnetite or mixed mineral contents of magnetite and antiferromagnetic minerals (Vidyasakar et al. 2015). Also, MUT area samples showed (Fig. 4) the B_{OCR} variation from 100 mT to 150 mT and in which some varies from 150 mT to 200 mT indicating the presence of antiferromagnetic

a.vidyasakar@gmail.com

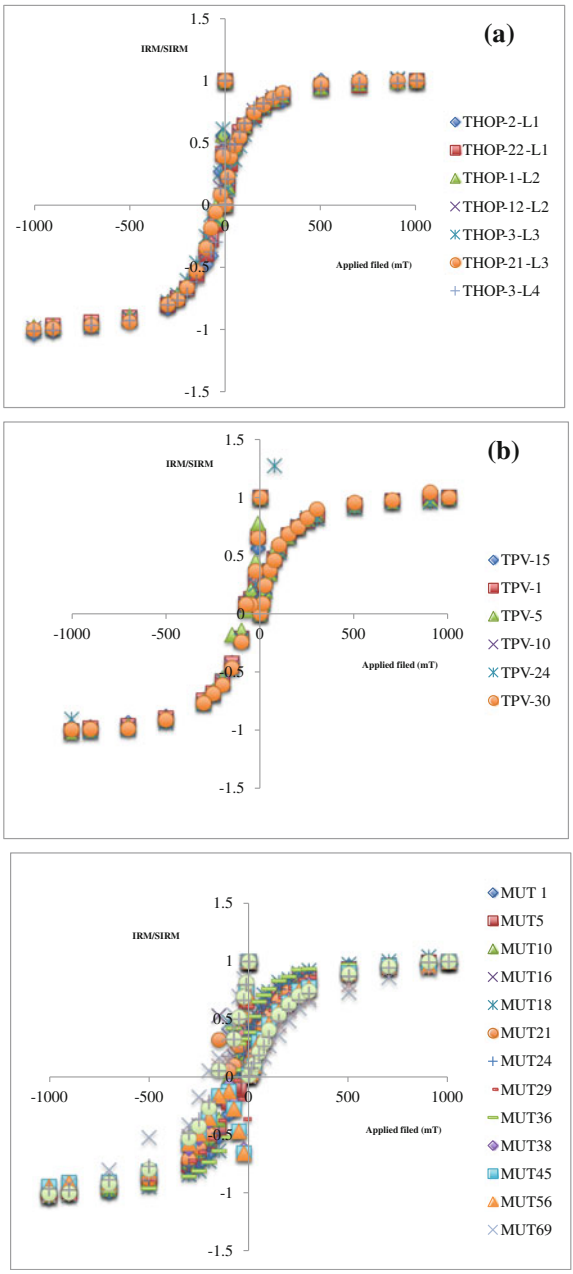

Fig. 4 IRM normalized (IRM/SIRM) acquisition curves for the representative samples from **a** THOP, **b** TPV and **c** MUT. THOP and TPV data source from Vidyasakar et al. (2015)

a.vidyasakar@gmail.com

minerals. Moreover, MUT area samples show B_{OCR} of <100 mT stating that they bear multidomain magnetite or mixed mineral contents of magnetite and antiferromagnetic minerals.

4.2 Variation of Magnetic Parameters

The depth changes and magnetic parameters of three profiles are presented in (Fig. 5). In THOP profile, at 220 cm one can see a decrease of χ, SIRM and S_{-300} and a slight increase of HIRM%. However, in TPV profile, χ and SIRM did not change with depth and seemed to be homogeneous till paleo-surface. Finally, in Muttom profile, there was a sudden increase of χ, SIRM, S_{-300} and S_{-100} at depths of 170, 350 and 390 cm and a steep decrease at depths of 200, 310, 370 and 410 cm respectively. It is obvious that below the depth of 400 cm at Muttom profile, there is no significant change in the profile.

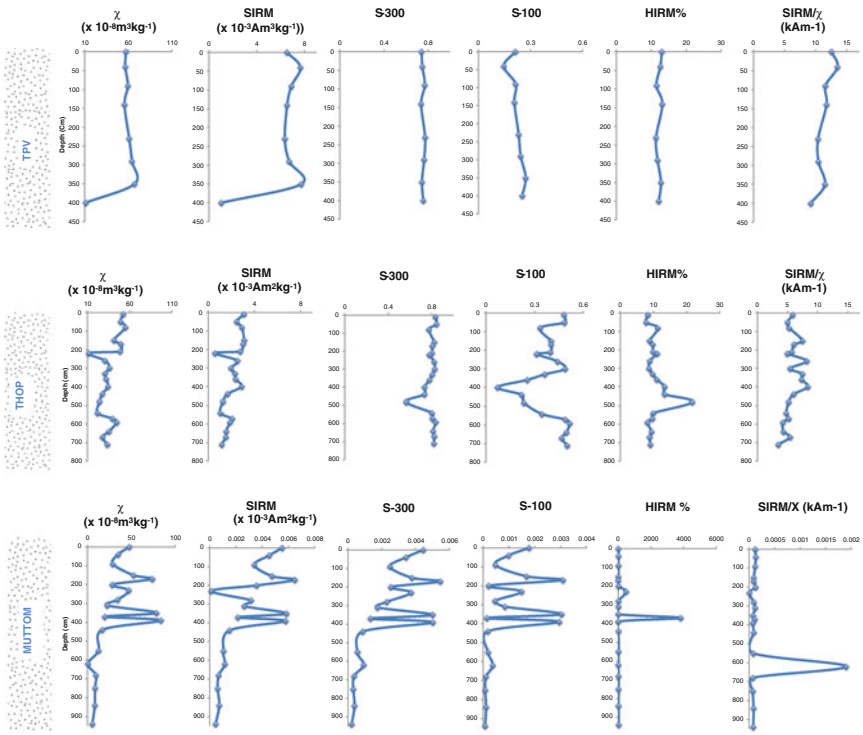

Fig. 5 Variation of magnetic parameters along each profile. TPV data source from Vidyasakar et al. (2015)

a.vidyasakar@gmail.com

4.3 Relationship Between Magnetic Parameters and Geochemical Data

In the analogy with geochemistry data, discrepancy of χ frequency hangs upon the deposition within the profile. The marine sediments are very subtle indicators of temporal variations in concentration and grain size of deposited terrigenous/lithogenous material. These sediments would have been deposited both in dry and wet periods and dependent on environment, concentration and grain size of deposition, which may have led to their deposition. By relating both the parameters through depth wise, we could determine between dry and wet of the depositional depth.

The TPV section (Fig. 6) indicated χ variations for the whole section seem to be nearly uniform with little variations towards end depth of 370 cm because of $CaCO_3$ cementation. It is to be noted that other than sand and clay (%) persists more or less uniform with minimal fluctuations in between, which are predominantly at the depth of 50 cm. The Fe (%) appears to be uniform till the depth and high-value variations in the last sample (350 cm) may be because of $CaCO_3$ cementation. Thus, THOP is the one section that showed a heterogeneous deposition from 220 to 330 cm (Fig. 6) because of shell fragments and calcrete cementation. Invariably as it is evident from (Fig. 6) there is a sharp decline in χ values from 220 to 330 cm, which is because of high values of $CaCO_3$ (%). At the depth of 550 cm, there is an increase in sand%, decrease in $CaCO_3$ (%) values and increase in χ values. Notably, clay has a steady rise when there is a downfall in the variation of sand%. Fe (%) contents have no big fluctuation till the depth of 200 cm however a sudden rise occurs till the depth of 600 cm, and then the values return to the initial ones. This may be due the sudden sea level changes during the time deposition and oxidation process combined with high wind energy could be responsible for the fluctuation.

In the Muttom section, χ values fluctuate in accordance with sand (%) until 400 cm and from 410 cm onwards χ values remain the same. The reason for this can be attributed to homogeneous concentration in the deposition. Moreover, at a depth of 430 cm, there is an increase in sand % and a decrease in clay % values. Thus, clay seems to have a steady increase when there is a downfall in a variation of sand %. $CaCO_3$ (%), OM (%) and Fe (%) have related fluctuation till 180 cm; particularly Fe (%) and $CaCO_3$ (%) have similar fluctuations throughout the profile.

The geochemical data with magnetic parameters and Spearman's rank correlation coefficients were determined to explore the possible relationship (Table 2). The correlation between SIRM and χ has been found significant ($P < 0.05$) in THOP and MUT sections and showed a perfect positive correlation with TPV section. The correlation between $CaCO_3$ and χ is negative in THOP and TPV sections (Vidyasakar et al. 2015). As expected, in MUT section, HIRM% and S_{-300} present significant ($P < 0.05$) negative correlation. In MUT section, S ratios and χ showed significant ($P < 0.05$) positive correlation. The $CaCO_3$ and S ratios showed

a.vidyasakar@gmail.com

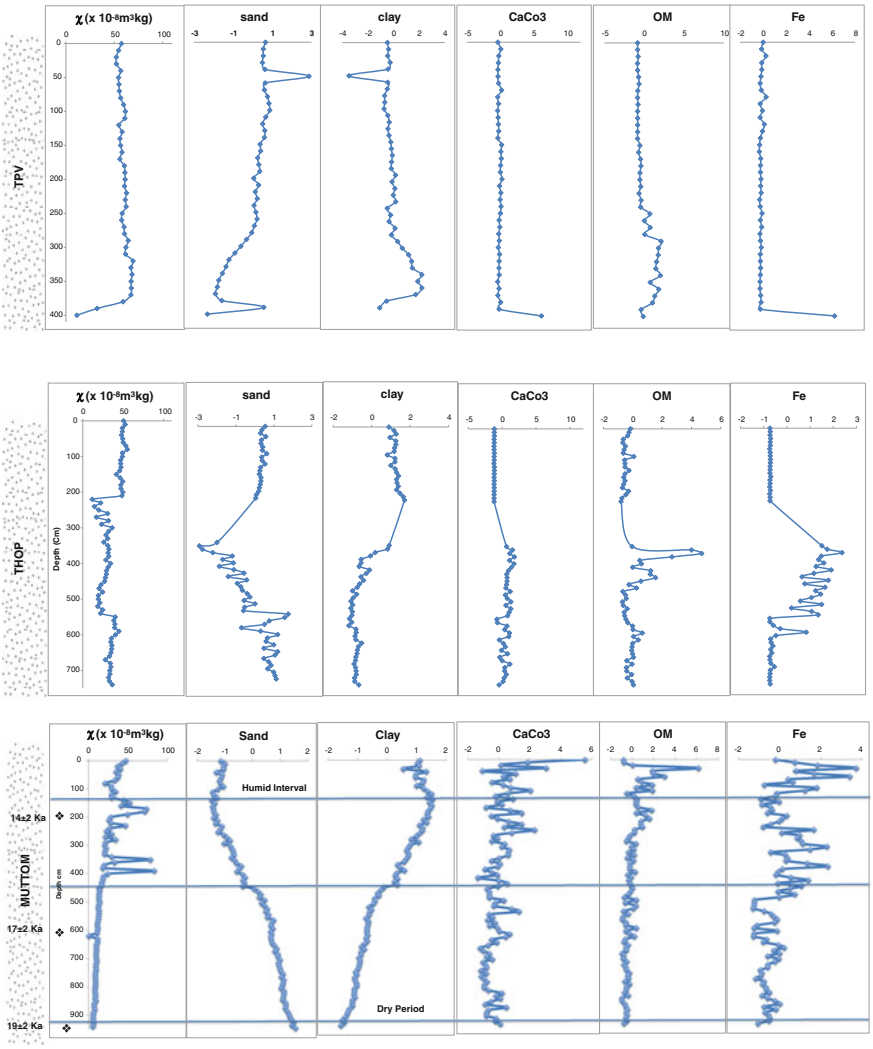

Fig. 6 Variation of magnetic susceptibility, sand%, clay%, CaCO3%, Fe% and OM (normalized values) along each profile. OSL dates in MUT section along with humid and dry period line. THOP and TPV data source from Vidyasakar et al. (2015)

significant ($P < 0.05$) negative correlation in THOP and negative correlation in TPV section. In these three sections, no significant correlation was found between OM and χ. In all the sections, the correlation between χ and clay is significant ($P < 0.05$). In MUT section, sand and S ratios showed significant negative and positive correlations with silt and χ respectively. In MUT section, OM showed positive correlation with clay and negative correlation with sand.

a.vidyasakar@gmail.com

Table 2 Spearman's rank correlation coefficients for geochemical data and magnetic parameters THOP, N = 20; MUT, N = 19 and TPV, N = 8)

	χ	SIRM	S-300	S-100	HIRM%	SIRM/X	Clay	Sand	Silt	OM	Fe	$CaCO_3$
MUT												
χ	1.0000											
SIRM	0.840*	1.0000										
S-300	0.956*	0.872*	1.0000									
S-100	0.953*	0.801*	0.923*	1.0000								
HIRM%	−0.1083	−0.1238	−0.1212	−0.1757	1.0000							
SIRM/χ	−0.3125	−0.1663	−0.1933	−0.1465	−0.0588	1.0000						
Clay	0.677*	0.723*	0.791*	0.546*	0.0221	−0.2248	1.0000					
Sand	−0.668*	−0.715*	−0.783*	−0.534*	−0.0349	0.2246	−0.999*	1.0000				
Silt	0.519*	0.4359	0.4104	0.3946	0.2190	−0.2840	0.4232	−0.4362	1.0000			
OM	0.1832	0.2552	0.3231	0.0613	−0.0562	−0.0848	0.620*	−0.622*	0.0091	1.0000		
Fe	0.2165	0.3117	0.2067	0.1095	0.3588	−0.3034	0.4806	−0.4853	0.3373	0.1131	1.0000	
$CaCO_3$	0.0788	0.1258	0.2304	0.1232	0.0171	0.0959	0.2152	−0.2301	−0.0607	−0.2185	−0.0603	1.0000
THOP												
χ	1.0000											
SIRM	0.750*	1.0000										
S-300	0.4260	0.1830	1.0000									
S-100	0.4080	−0.0600	0.836*	1.0000								
HIRM%	−0.4260	−0.1830	−1.000*	−0.836*	1.0000							
SIRM/χ	0.0560	0.672*	−0.1800	−0.504*	0.1800	1.0000						
Clay	0.625*	0.729*	0.0570	−0.2540	−0.0570	0.571*	1.0000					
Sand	0.2210	−0.0430	0.4390	0.564*	−0.4390	−0.3250	−0.1890	1.0000				
Silt	−0.2040	−0.4290	0.4390	0.7060	−0.4390	−0.552*	−0.4900	0.3880	1.0000			
OM	−0.0320	−0.1050	−0.0450	0.1340	0.0450	−0.2180	−0.4430	−0.0430	0.3630	1.0000		

(continued)

a.vidyasakar@gmail.com

Table 2 (continued)

	χ	SIRM	S-300	S-100	HIRM%	SIRM/X	Clay	Sand	Silt	OM	Fe	$CaCO_3$
MUT												
Fe	−0.543*	−0.486*	−0.475*	−0.3210	0.475*	−0.2360	−0.486*	−0.5360	0.0910	0.490*	1.0000	
$CaCO_3$	−0.657*	−0.479*	−0.2860	−0.0790	0.2860	−0.1500	−0.725*	−0.4000	0.2910	0.527*	0.654*	1.0000
TPV												
χ	1.0000											
SIRM	0.5000	1.0000										
S-300	0.3330	0.1830	1.0000									
S-100	0.4760	−0.0600	0.3100	1.0000								
HIRM%	−0.3330	−0.183 0	−1.000*	−0.3100	1.0000							
SIRM/χ	−0.143 0	0.672*	−0.6190	−0.762*	0.6190	1.0000						
Clay	0.738*	0.729*	0.0000	0.2620	0.0000	−0.1190	1.0000					
Sand	−0.0950	−0.0430	−0.0480	−0.762*	0.0480	0.762*	−0.3100	1.0000				
Silt	0.0480	−0.4290	−0.3100	0.5710	0.3100	−0.3330	0.1190	−0.741*	1.0000			
OM	0.5480	−0.1050	0.5000	0.833*	−0.5000	−0.786*	0.3810	−0.738*	0.5950	1.0000		
Fe	−0.667 0	−0.486*	−0.3570	−0.1900	0.3570	0.1900	−0.741*	−0.0480	0.1900	−0.2380	1.0000	
$CaCO_3$	−0.262 0	−0.479 *	0.738*	0.2140	−0.738*	−0.738*	−0.3330	−0.3100	−0.1190	0.3810	0.1430	1.0000

Values are significant at $*p < 0.05$

THOP and TPV data source from Vidyasakar et al. (2015)

a.vidyasakar@gmail.com

4.4 Principal Component Analysis (PCA) 33

In PCA correlation, X-ray diffraction data was used to find out the similar type of mineral deposition in sampling section. This would help us to get an idea about the deposition between Southeast coast and southwest cost of a sampling area. At 940 cm depth, Muttom sample (Table 3) had 81% correlation between Edayanvillai (TPV) at the depth of 230–330 cm. Moreover, TPV had showed 84% positive correlation between 10 and 230 cm. The PCA correlation confirmed that TPV and MUT almost have a similar type of mineral deposition. Interestingly, THOP did not showed positive correlation with MUT and TPV. Muttom had 88% positive correlation between 180 and 350 cm respectively. Surprisingly, THOP have not showed any positive correlation with PCA. This correlation analysis indicated that THOP may have gone through ample wash over during the rise in sea level or a seasonal Arroyo/Gulch (Fig. 3) could have taken place over deposition. It is to be noted that THOP is the only sample that is pale yellow compared to TPV and MUT samples, which are darker red.

4.5 Mineral Inference with XRD Analysis

The present research study used X-ray diffraction as a tool to find out the minerals and its percentage of available quantity at different depths. In doing so, one can roughly determine the type of deposition that has taken place and its occurrence. In TPV section (Table 4), quartz, rutile, zircon, kaolinite, hematite, magnetite and sillimanite are present. In this section, presence of quartz is dominant than other minerals. The minerals that are present in TPV section are usually found in semi-arid/dry condition. The Aeolian process must have also made a significant role during the TPV deposition. In THOP section, quartz, calcite, rutile, zircon, pyrope and sylvite are present. At 30 cm, the minerals are supported by Aeolian process, which showed arid deposition with heavy wind flow. Furthermore, at 280 cm, calcite mineral depicted the dominance due to shells of dead marine organisms. This supported the presence of paleo minerals (pyrope and sylvite) in abundance in the sea level at a depth of 510 cm. These minerals were formed during dry condition. Also, in MUT section (Table 4) quartz, almandine, kaolinite, hematite, and halloysite are present. In this section, hematite and kaolinite are dominant among other minerals. These minerals are formed during wet-to-dry period. This may be because of ancient paleo sea level or due to primordial lagoon formation. Thus, during Last Glacial Maximum (LGM), continental shelves were wide-open with a vast reservoir of sediments with strong landward winds during (NE) winter monsoon and sediments coasted inland until 11.4 ka to form coastal aeolian teri deposits. The Coastal teri reddening happened by in situ weathering that started at <11.4–5.6 ka during a humid climate (Jayangondaperumal et al. 2012).

a.vidyasakar@gmail.com

Table 3 PCA correlation between section depositions

Samples	TPV41	TPV24	TPV1	MUT95	MUT36	MUT19	THOP20_ L4	THOP18_L3	THOP7_L2	THOP4_L1
TPV41	100	34	34	35	29	27	48	44	54	37
TPV24	34	100	84	81*	66	69	58	34	34	55
TPV1	34	84	100	79	67	69	56	35	33	53
MUT95	35	81*	79*	100	65	67	65	37	37	57
MUT36	29	66	67	65	100	88*	49	24	26	38
MUT19	27	69	69	67	88*	100	46	26	28	41
THOP20_ L4	48	58	56	65	49	46	100	47	46	60
THOP18_L3	44	34	35	37	24	26	47	100	54	59
THOP7_L2	54	34	33	37	26	28	46	54	100	43
THOP4_L1	37	55	53	57	38	41	60	59	43	100

* Positive correlation

a.vidyasakar@gmail.com

Table 4 List of minerals found by XRD analysis in various sections at different depth

Ref.no	Depth/min	Quartz	Calcite	Rutile	Zircon	Pyrope	Almandine	Sylvite	Kaolanite	Hematite	Halloysite	Xenotime	Ilmenite	Magnesite	Sillmanite	Magnetite
TPV1	0 CM	✓	X	✓	✓	X	X	X	✓	✓	X	X	X	✓	X	X
TPV24	230 cm	✓	X	X	✓	X	X	X	✓	✓	X	X	X	X	✓	X
TPV57	560 cm	✓	✓	✓	X	X	X	X	X	✓	X	X	X	X	X	X
THOP/L1/4	30 cm	✓	X	✓	✓	X	✓	X	X	X	X	X	X	X	X	X
THOP/L2/7	280 cm	✓	✓	✓	X	X	X	X	X	X	X	X	X	X	X	X
THOP/L3/18	510 cm	✓	✓	✓	X	✓	X	✓	X	X	X	X	X	X	X	X
THOP/L4/20	740 cm	✓	✓	✓	✓	X	X	X	X	X	X	X	X	X	X	X
MUT'19	180 cm	✓	X	X	X	X	✓	X	✓	✓	✓	✓	X	X	X	X
MUT36	350 cm	✓	X	X	X	X	X	X	✓	✓	X	X	X	X	X	X
MUT95	940 cm	✓	X	X	X	X	✓	X	X	✓	✓	X	X	X	X	X

THOP and TPV data source from Vidyasakar et al. (2015)

a.vidyasakar@gmail.com

4.6 Depositional Period—OSL Chronology

Coastal depositions are very sensitive to the environment and have a particular capacity to store the untold story of the period/inference in deposition. Therefore, with limited resources (Fig. 6) the researchers have compared χ, Sand%, Clay%, $CaCO_3$%, OM% and Fe% with each other to draw a distinct line between dry and wet periods. Muttom section (Fig. 6) has three OSL dates, which would let us know the approximate age of deposition in accordance with depth. The previous terrestrial record (Table 5) from this region supported the line drawn between the humid and dry period in this section.

According to Folk (1976) red beds are developed from minerals having source of abundant iron, either heavy minerals or ferruginous clays. They are mostly originated from heavy minerals when deposited above the water table for easier access to Oxygen.

4.7 Comparison Between Magnetic Parameters and XRD Analysis

In XRD analysis, we have determined various minerals that are present at different depths. In Table 4 one can see that magnetite is not present in any of the following samples. However, magnetic parameters such as remanence coercivity (Fig. 3) were able to pick minor quantities of magnetite present in the samples. The presence of magnetite could not be assessed by XRD due to its less availability in the sample, which implied magnetic measurements are more precise and faster than X-ray diffraction as per the magnetic mineralogy studies.

Table 5 Previous terrestrial climate records in India

Epoch	Time interval (Ka)	Climatic proxy/method	Location	Inference	Reference
Late Pleistocene–Early Holocene	14.5–7	Pollen	Berijam lake, Palani Hills, S. India	Warm and humid climate	Bera et al. (1995)
	16	$S1^3$ C of peat	Nilgiri Hills, S. India	Arid condition	Rajagopalan et al. (1997)
	20–17	Pollen	Berijam lake, Palani Hills, S. India	Cold and dry climatic condition	Bera et al. (1995)
	20–11.0	OSL dating	S.margin of Thar Dessert	Dry climatic condition	Juyal et al. (2006)

a.vidyasakar@gmail.com

5 Discussion

- Magnetic parameters showed the significant contribution of canted antiferromagnetic (hematite) structures to sands. In adherence to the findings of Gardner (1981) on Teri sands, hematite originated from chemical alteration of ilmenite and garnet. Thus indicated wet, humid climate and high temperature due to oxidation of magnetite.
- The remanence coercivity parameter B_{OCR} indicated in TPV samples indicated the presence of a multidomain magnetite or mixed mineral contents of magnetite and antiferromagnetic minerals. Finally, some THOP samples showed B_{OCR} indicating multidomain magnetite or magnetite and antiferromagnetic minerals. In other THOP samples presence of B_{OCR} confirmed that these minerals are magnetite bearing. The presence of a magnetite-structure in THOP and TPV samples supported values of S_{-300} close to unity, 0.79 and 0.75, respectively. The presence of magnetite was however not detected by X-ray diffraction, even so magnetic measurements point out the ferromagnetic behavior of THOP and TPV samples.
- The MUT samples showed the highest quantity of hematite and smallest quantity of magnetite as indicated by highest values of HIRM% and lowest of S_{-300} and SIRM respectively.
- The SIRM and χ have showed positive correlations with MUT, THOP and TPV sections due to the magnetic signal of ferromagnetic minerals. The negative correlations between $CaCO_3$ and χ in THOP and TPV sections are justified by diamagnetism of carbonaceous materials. The HIRM% and S_{-300} are found negative and has a significant correlation in all sections, which has been described using the fact that first parameter is associated with the existence of antiferromagnetic minerals and second with ferromagnetic minerals. There were no correlations found between Fe (%) and χ in MUT and TPV sections, which has been quite surprising. However, this may be related to the fact that whole content of Fe was determined instead of FeO and Fe_2O_3 contents, which may correlate with magnetite and hematite content. Also, OM and χ have no significant correlation, which is a bit strange, but this has been justified in accordance with Lourenço et al. (2014). The positive correlation between χ with clay in TPV, THOP and MUT sections, based in Spearman correlation, lead to magnetic susceptibility, which has been dominantly meticulous by differences in the concentration of ferromagnetic minerals and paramagnetic minerals carried by clay matrix.
- The mean SIRM/χ value of 5.78 kA m^{-1} recorded in the present study in THOP section indicated the average grain size of ferromagnetic particles of ca is 8 μm.
- The presence of magnetite in THOP (near coastal) and TPV sections are probably due to oceanic origin (biogenic magnetite particles), which has been carried away by strong offshore winds (Vidyasakar et al. 2015). Also, the

a.vidyasakar@gmail.com

presence of biogenic magnetite in sediments was mentioned by several authors (Kirschvink and Chang 1984).

- XRD investigation showed the minerals that exist in TPV section are commonly found to be in semi-arid/slow dry conditions.
- XRD proves that Aeolian process must have played a significant role in TPV deposition.
- In XRD analysis, THOP section at 280 cm depicted calcite mineral is dominant due to shells of dead marine organisms. It also supported the presence of paleo minerals (pyrope and sylvite) in abundance in the sea level at a depth of 510 cm. However, these minerals were formed during dry conditions.
- PCA correlation showed TPV and MUT sections have a similar type of depositions. Also, THOP have not showed any positive correlation with PCA. The correlation analysis indicated that THOP area would have gone through several wash over during rise in sea level or storm surge being nearer to coastal belt, hence, showed negative correlations.

6 Conclusion

The investigation in connection with features of magnetic parameters and its association with OSL, X-ray diffraction and geochemistry data made the subsequent conclusions possible:

- The studied sections of Teri sands show significant contribution of hematite presence due to oxidation of magnetite.
- In MUT, $\sim 14 \pm 2$ ka depositions showed the humid interval at $\sim 17 \pm 2$ to $\sim 19 \pm 2$ ka, which displays depositions during the dry period.
- In TPV, aeolian process played a significant role and the minerals that are found in that section are usually formed in Semi-arid/Dry condition.
- The three sections of XRD data were correlated with each other and found that MUT and TPV have a similar type of deposition. Moreover, THOP may have gone through a wash during some natural calamities or Arroyo/Gulch would have occurred.
- It has been a fact that during the Last Glacial Maximum (LGM) continental shelves were exposed to a vast reservoir of sediments with strong landward winds (NE/E) to form aeolian teri. The NE winter monsoon forms the fluvial teri sediments.
- The SW summer monsoon also plays a vital role in carrying sediments from one place to another, but it depends on the availability of loose sediments (minerals) at the time of transport.
- The colour red in the sediments is a distinct indicator of climate that prevailed at the time of diagenetic/pedogenetic transformation.

a.vidyasakar@gmail.com

Acknowledgements The researchers are thankful to Dr. Ana Lourenço for their valuable advice and comments during the work. We are very thankful to Indian Journal of Geo-Marine science (IJMS) by allowing us to use the few images and tables from their journal. Special thanks to Ms. Sujita Ganaraj for her support in documentation assistance and Mr. Arul Britto for their timely during sample collection in this distinct field. Lastly, acknowledgements to Erasmus Mundus (INDIA4EU ll) scholarship officials for their continuous financial support to the research study of Mr. Vidyasakar Anburaj (Indi1200057) during 2013–2015.

References

Aitken MJ (1998) Introduction to optical dating. Oxford University Press, Oxford 262

Alagarsamy R (2009) Environmental magnetism and application in the continental shelf sediments of India. Mar Environ Res 68:49–58

Alappat L, Palaniandy S, Shukla AD, Trivikramji KP, Singhvi AK (2013a) Chronology of red dune aggradations of South India and its paleo-environmental significance. Geochronometria 40(4):274–282

Alappat L, Morthekai P, Vidyasakar Srinivasalu S, Sandode SJ, Reddy DV, Singhvi AK (2013b) Chronology of deposition of coastal Red dunes (Teri sands) in south India and its paleoenvironmental implictions. PAGES-YSM, Goa (O)

Alappat L, Frechen M, Kumar SS, Babu DSS, Ravurb R, Tsukamotoa S (2015) Evidence of late Holocene shoreline progradation in the coast of Kerala, South India obtained from OSL dating of palaeo-beach ridges. Geomorphol 245:73–86

Albarède F (2003) Geochemistry: an introduction. Cambridge University Press, p 356

Blatt H, Middleton G, Murray R (1980) Origin of sedimentary rocks. Prentice-Hall, Englewood Cliffs, p 782

Bera SK, Gupta HP, Farooqui A (1995) Berijam Lake. 20,000 yrs. Sequence of paleofloristics and paleoenvironment in Palni Hills, South India. Geophytology 26:99–104

Brückner H (1988) Indicators for formerly high sea levels along the east coast of India and on the Andaman Islands. Hamburger Geographische Studien 44:47–72

Brückner H (1989) Late quaternary shorelines of India. In: Scott DB (ed) Late Quaternary sea level correlation and applications. Kluwer Academic, New York, pp 169–194

Chandrasekharan S, Murugan C (2001) Heavy minerals in the beach and the coastal red sands (Teris) of Tamilnadu. Special issue on Beach and Inland Heavy Mineral Sand Deposits of India, Exploration and Research for Atomic Minerals 13:87–109

Dekkers MJ (1997) Environmental magnetism: an introduction. Geol Mijnbouw 76:163–182

Evans ME, Heller F (2003) Environmental magnetism. Academic Press, p 213

Folk RL (1976) Reddening of desert sands; Simpson Desert, N.T., Australia. J Sedim Res 46 (3):604–615

Gardner RAM (1981) Reddening of dune sands—evidence from southeast India. Earth Surf Proc Land 6:459–468

Gardner RAM (1986) Quaternary coastal sediments and stratigraphy Southeast India. Man Environ X, 51–72

Guérin G, Mercier N, Adamiec G (2011) Dose-rate conversion factors: update. Ancient TL 29:5–8

Islam MS, Tooley MJ (1999) Coastal and sea-level changes during the Holocene in Bangladesh. Quat Int 55:61–75

Jacobs Z, Wintle AG, Roberts RG, Duller GAT (2008) Equivalent dose distributions from single grains of quartz at Sibudu, South Africa: context, causes and consequences for optical dating of archaeological deposits. J Archaeol Sci 35:1808–1820

Jayangondaperumal R, Murari MK, Sivasubramanian P, Chandrasekar N, Singhvi AK (2012) Luminescence dating of fluvial and coastal red sediments in the SE coast, India, and implications for paleoenvironmental changes and dune reddening. Quat Res 77(3):468–481

a.vidyasakar@gmail.com

Joseph S, Thrivikramaji KP, Anirudhan S (1997) Textural parameters, discriminant analysis and depositional environments of the Teri sands, southern Tamil Nadu. J Geol Soc India 50 (3):323–329

Joseph S, Thrivikramji KP, Anirudhan S (1999) Mud content, clay minerals and oxidation states of iron in Teris of southern Tamil Nadu. Implication to the origin of redness. J Indian Assoc Sedimentol 18:83–94

Juyal N, Chamyal LS, Bhandari S, Bhushan R, Singhvi AK (2006) Continental record of the southwest monsoon during the last 130 ka: evidence from the southern margin of the Thar Desert, India. Quat Sci Rev 25(19–20):2632–2650

Kirschvink JL, Chang SBR (1984) Ultrafine–grained magnetite in deep-sea sediments: Possible bacterial magnetofossils. Geology 12:559–562

Lapa ML, Reis RP (1977) Contribuicâo para o estudo dos minerais argilosos em formações sedimentares da Orla Meso-Cenozóica Ocidental. Memórias e Notícias, Pub Mus Lab Min Geol Univ Coimbra 83:3–25

Lourenço AM, Rocha F, Gomes CR (2012) Relationships between magnetic parameters, chemical composition and clay minerals of topsoils near Coimbra, central Portugal. Nat Hazards Earth Syst Sci 12:2545–2555

Lourenço AM, Sequeira E, Sant'Ovaia H, Gomes CR (2014) Magnetic, geochemical and pedological characterisation of soil profiles from different environments and geological backgrounds near Coimbra, Portugal. Geoderma 213:408–418

Maher BA (1986) Characterisation of soils by mineral magnetic measurements. Phys Earth Plan Int 42:76–92

Maher BA, Thompson R (1999) Quaternary climates, environments and magnetism. Cambridge University Press, 390 p

Mejdahl V (1979) Thermoluminescence dating. Beta dose attenuation in quartz grains. Archaeometry 21:61–63

Moreno E, Sagnotti L, Dinare's-Turell J, Winkler A, Cascella A (2003) Biomonitoring of traffic air pollution in Rome using magnetic properties of tree leaves, Atmos Environ 37:2967–2977

Morner Nils-Axel (2010) Some problem in the reconstruction of mean sea level and its changes with time. Quat Int 221:3–8

Murray AS, Wintle AG (2000) Luminescence dating of quartz using an improved single-aliquot regenerative-dose protocol. Radiat Meas 32:57–73

Peel MC, Finlayson BL, McMahon TA (2007) Updated world map of the KÖppen-Geiger climate classification. Hydrol Earth Syst Sci Discuss 4(2):439–473

Prescott JR, Hutton JT (1994) Cosmic ray contributions to dose rates for luminescence and ESR dating. Large depths and long-term time variations. Radiat Meas 23:497–500

Rajagopalan G, sukumar R, Ramesh R, Pant RK, Rajagopalan G (1997) Late quaternary vegetational and climate changes from tropical peats in southern India—an extended record up to 40000 years BP. Curr Sci 73(1):60–63

Sanchez Goñi MF, Harrison SP (2010) Vegetation response to millennial-scale variability during the last glacial. Quat Sci Rev Spec 29:2823–2980

Sandgren P, Thompson R (1990) Mineral magnetic characteristics of podzolic soils developed on sand dunes in the Lake Gosciaz catchment, central Poland. Phys Earth Planet Inter 60:297–313

Saravanan P (2012) Depositional characteristics of recent and past washover sand sheets from cauvery delta coast, Tamil Nadu, India. PhD thesis. Anna University

Thompson R, Oldfield F (1986) Environmental magnetism. Allen & Unwin Press, London, p 227

Verosub KL, Roberts AP (1995) Environmental magnetism: Past, present, and future. J Geophys Res 100(B2):2175–2192

Vidyasakar A, Sant'Ovaia H, Gomes CR, Lourenço AM, Srinivasalu S (2015) A Magnetic and Geochemical Characterization of Red Dune Sands (teri sands) of Tamil Nadu coast. Indian J Mar Sci 44(9):1382–1392

a.vidyasakar@gmail.com

Wintle AG, Murray AS (2006) A review of quartz optically stimulated luminescence characteristics and their relevance in single-aliquot regeneration dating protocols. Radiat Meas 41(4):369–391

Wolff EW, Chappellaz J, Blunier T, Rasmussen SO, Svensson A (2010) Millennial-scale variability during the last glacial: the ice core record. Quat Sci Rev 29:2828–2838.

http://en.climate-data.org

a.vidyasakar@gmail.com